PNAS
www.pnas.org

Supplementary Information for

Structures of ligand occupied β-klotho complexes reveal molecular mechanism underlying endocrine FGF specificity and activity

Ekaterina S. Kuzina, Peter Man-Un Ung, Jyotidarsini Mohanty, Francisco Tome, Jungyuen Choi, Els Pardon, Jan Steyaert, Irit Lax, Avner Schlessinger, Joseph Schlessinger* and Sangwon Lee*

*For correspondence:
Joseph Schlessinger and Sangwon Lee
Email: joseph.schlessinger@yale.edu (J.S.), s.lee@yale.edu (S.L.)

This PDF file includes:

Supplementary Methods
Figs. S1 to S7
Tables S1 to S2
Captions for movies S1
References for SI reference citations

Other supplementary materials for this manuscript include the following:

Movies S1

www.pnas.org/cgi/doi/10.1073/pnas.1822055116

Supplementary Methods

Plasmid construction

pCEP4 vector containing sequence for Fc region of human IgG1 fused to human β-Klotho amino acids 30-983 (sKLB) was created as described previously (1). cDNA region encoding for amino acids 25-216 of human FGF19 or codon-optimized DNA encoding for amino acids 25-209 of human FGF21 harboring three mutations, L126R, P199G, A208E, were subcloned into pET28a vector. Plasmids of FGF19 and FGF21 point mutants were generated by following standard site-directed mutagenesis protocol using plasmids containing WT FGF19 or prFGF21. FGF19 and FGF21 variants with altered site 2 were generated by amplification of FGF19 and FGF21 genetic constructs using extended 3' primers. Genetic constructs encoding for FGF19 variants with site1 and site 2 from FGF21 were ordered from BlueHeron Biotech, LLC.

Protein expression and purification

sKLB containing mutations on two N-glycosylation sites, N308Q/N611Q, FGF21 and nanobodies were expressed and purified as described previously (1). For expression of FGF19 or its variants, plasmids were transformed into BL21-Gold (DE3) competent cells. Transformants were grown in LB medium containing 50 μg/mL kanamycin, shaking at 240 rpm at 37˚C. Bacteria were induced with 1 mM IPTG for 4 hours at 37˚C and washed inclusion bodies were solubilized in a buffer (6 M guanidine hydrochloride, 50 mM Tris, 10 mM DTT, pH 8.0) for one hour at room temperature. The solubilization mixture was then added to refolding buffer (2 M guanidine hydrochloride, 20 mM Tris pH 8.0, 0.5 M arginine hydrochloride, 2mM reduced glutathione, 0.2mM oxidized glutathione), mixed and dialyzed against a dialysis buffer (20 mM Tris pH 8.0, 500mM

NaCl, 10% glycerol) for 18 hours at 4°C. The resulting solution containing N-terminal hexa-histidine-tagged FGF19 was supplemented with 10 mM imidazole and incubated with Ni-NTA agarose (Qiagen) for 1 hr at 4˚C. The resin was washed with 20 column volume of dialysis buffer containing 10 mM imidazole, and the protein was eluted from the resin with dialysis buffer containing 300 mM imidazole. The protein solution was injected into HiLoad 26/600 Superdex 200 (GE Healthcare) size exclusion chromatography column equilibrated with 20 mM Tris-HCl, 900 mM NaCl at pH 8.0. The eluted fractions containing FGF19 were pooled, concentrated to 3 mg/mL, flash-frozen, and stored at -80˚C until further study.

For generating GST-FGF21$_{CT}$ and GST-FGF19$_{CT}$, DNA sequences encoding either amino acids 169-209 of FGF21 or amino acids 167-216 of FGF19 were cloned into pGEX-4T-1 vector (GE Healthcare), and the plasmid was transformed into BL21-Gold (DE3) competent cells (Agilent Technologies). Transformants were grown in LB media containing 100 μg/mL ampicillin at 37˚C until A600 reached 0.6, and induced with 1 mM IPTG for 4 hours at 37˚C. Bacte were collected, lysed in PBS using EmulsiFlex-C3 homogenizer (Avestin, Inc.), and centrifuged at 20,000 ×g for 30 minutes at 4˚C. The supernatant containing GST-FGF21$_{CT}$ or GST-FGF19$_{CT}$ was incubated with Glutathione Sepharose 4B (GE Healthcare) pre-equilibrated with PBS, for 1 hour at 4˚C. The beads were washed with 50 column volume of PBS and the protein was eluted with 20 mM HEPES, 150 mM NaCl, 10 mM reduced glutathione, pH 7.3. The fusion proteins were further purified by size-exclusion chromatography on Superdex S200 column in 20 mM HEPES, 150 mM NaCl before flash frozen and stored at -80˚C.

Bio-Layer Interferometry (BLI) measurements

Binding affinities and kinetic values of interactions between β-Klotho and various forms of FGF19 or FGF21 were studied using Bio-Layer Interferometry (BLI). Octet RED96 system (Pall FortéBio) equipped with HIS1K Biosensor probes was used to perform all BLI experiments. Biosensor tips were loaded with hexa-histidine-tagged FGF19, FGF21 or their variants at 10 μg/ml for 60sec. Alternatively, anti-GST biosensor tips were loaded with GST fused with either $FGF19_{CT}$ or $FGF21_{CT}$. Subsequently, ligand-loaded sensor tips were dipped into microplate wells containing sKLB in series of concentrations, ranging from 6.25 nM to 400 nM in 2-fold dilutions in 20 mM HEPES, 150 mM NaCl, pH 7.5, 0.01% Tween-20, 1 mg/mL BSA. The sensor tips were regenerated with 10mM glycine (pH 1.5) after each binding cycle. The collected data were referenced using a parallel buffer control subtraction, and sensograms were fitted globally to a 1:1 Langmuir binding model using FortéBio Data Analysis 10.0 software provided by the manufacturer. The kinetic rate constants (k_{on} and k_{off}) and the dissociation constant, K_D were determined for all interactions. All measurements were performed in at least 3 independent experiments and resulting S.E.M. were calculated for all parameters measured.

MicroScale Thermophoresis (MST) measurements

All MST measurements were performed using the Monolith NT.115Pico instrument (NanoTemper Technologies) with Monolith NT.115 MST Premium Coated Capillaries. Purified FGF21 or FGF19 were fluorescently labeled using the Monolith His-Tag Labeling Kit RED-tris-NTA (NanoTemper Technologies) according to the instruction provided by the manufacturer. Samples for binding affinity measurements were prepared by mixing 100 nM of fluorescently labeled FGF21 or FGF19 with a series of concentrations, ranging from 0.15 nM to 5000 nM in 2-fold dilutions, of purified sKLB

in 20 mM HEPES, 150 mM NaCl, pH 7.5, 0.1% Tween-20, 0.5 mg/mL BSA. The thermophoretic movements of labeled FGF21 or FGF19 in each sample were monitored (LED 20%, IR laser 20%,) and the normalized fluorescence intensities (FNorm) for each sample were plotted against the concentrations of sKLB. All the data were analyzed with the MO. Affinity Analysis software (NanoTemper Technologies) provided by the manufacturer.

Cellular activities of FGF mutants

L6 cells stably co-expressing either WT FGFR1c or WT FGFR4 together with WT β-Klotho with C-terminal HA-tag, were grown in DMEM supplemented with 10% FBS, 100 U/mL Penicillin-Streptomycin, 0.1 mg/ml hygromycin and 1 μg/ml puromycin in 100 mm-plates to 70% confluency. Cells were starved overnight in DMEM without FBS and stimulated for 10 minutes at 37˚C with ligands at indicated concentrations. Washed cells were lysed on ice-cold lysis buffer (25 mM Tris, pH 7.4, 150 mM NaCl, 1% Triton X-100, 1 mM EDTA, 1 mM sodium orthovanadate) with protease inhibitors (Roche). Lysates were mixed with 2xLaemmli sample buffer (Bio-Rad) and subjected to immunoblotting with either anti-phospho-MAPK or anti-MAPK antibodies.

Homology modeling of sKLA

MODELLER v9.17 (2) was used to generate homology model of sKLA, with two cycles of optimization, using the crystal structure of sKLB:FGF21$_{CT}$ complex (PDB ID: 5VAQ) as a template. The models were assessed with Z-DOPE (3), a normalized atomic distance-dependent statistical potential based on known protein structures. The best scoring models were subjected to optimization and minimization to optimize hydrogen-bond interactions and remove steric clashes, respectively, with Schrödinger's Protein

Preparation function (Schrödinger Suite 2017-1: Epik, Schrödinger, LLC, New York, NY). The electrostatic potentials were calculated with APBS (4) and PDB2PQR (5) implemented in PyMOL 1.7.2 (Schrödinger, LLC, New York, NY).

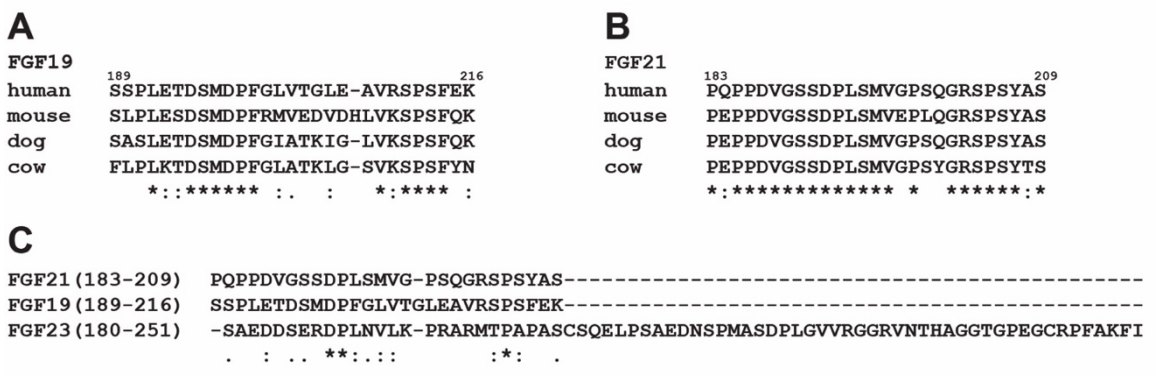

Fig. S1. Amino acid sequence alignments of the C-terminal regions FGF19, FGF21 and FGF23. Sequence alignments of (A) FGF19 or (B) FGF21 from different species. (C) Sequence alignments of human FGF19, FGF21 and FGF23. Amino acid numbers for human FGFs are indicated in (A) and (B).

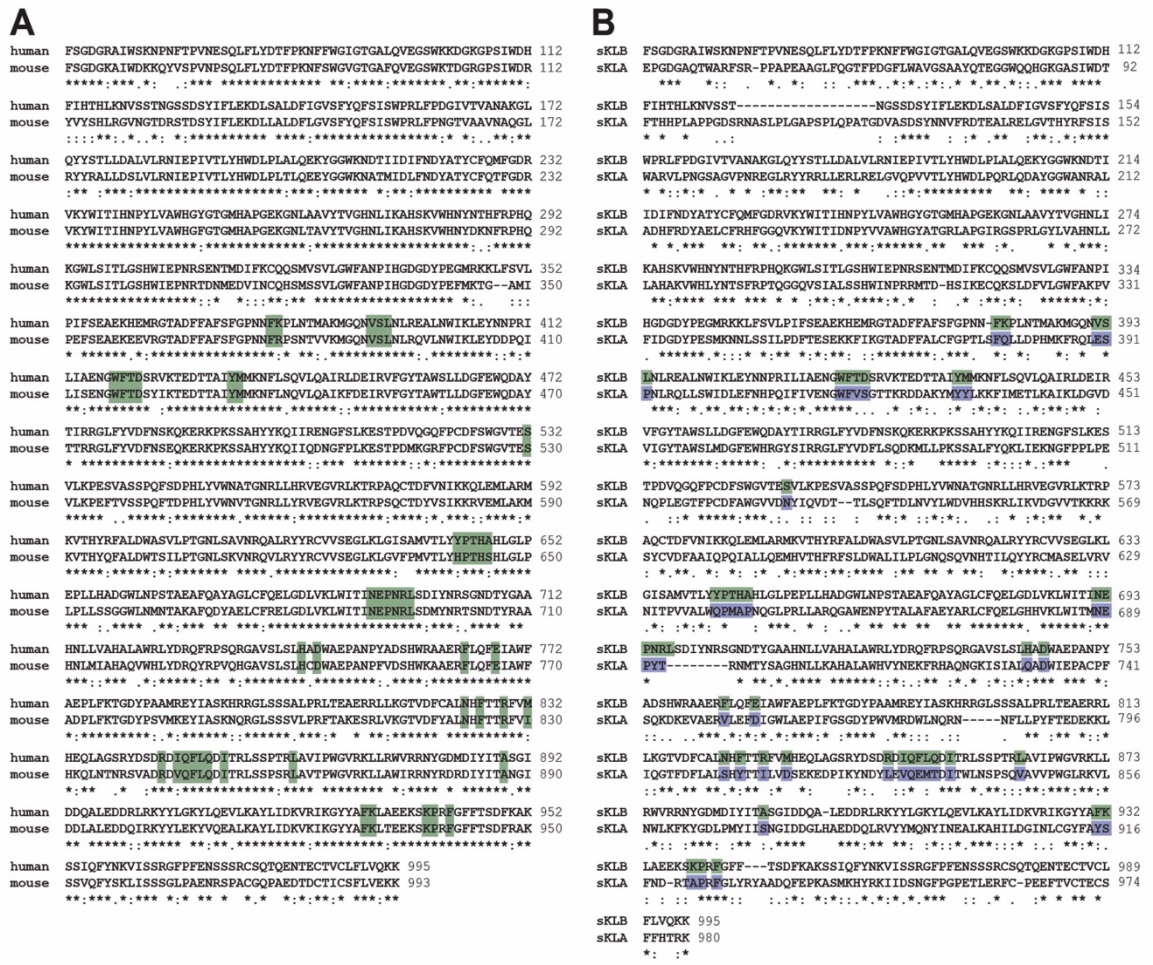

Fig. S2. Amino acid sequence alignments of the extracellular domains of Klotho proteins. Sequence alignments of the (A) extracellular regions of human β-Klotho and mouse β-Klotho, and sequence alignment of the (B) extracellular regions of human β-Klotho and human α-Klotho. Residues in human β-Klotho interacting with $FGF19_{CT}$ or $FGF21_{CT}$ identified in the crystal structures and corresponding residues in mouse β-Klotho and human α-Klotho are highlighted.

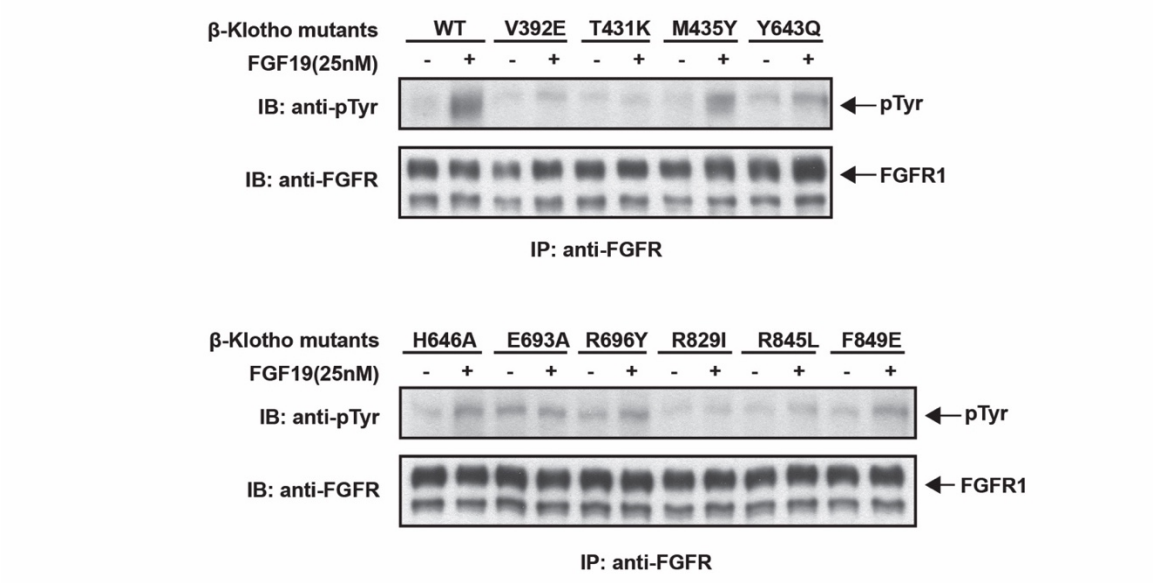

Fig. S3. FGF19 stimulation of tyrosine phosphorylation of FGFR1c in cells expressing WT or β-Klotho mutants. L6 cells co-expressing WT-FGFR1c and β-Klotho harboring mutations in the ligand-binding sites were stimulated with WT-FGF19 and analyzed for FGFR1c activation by monitoring tyrosine phosphorylation of FGFR1c. Lysates of ligand stimulated or unstimulated cells were subjected to immunoprecipitation with anti FGFR1 antibodies followed by immunoblotting with either anti-pTyr or anti-FGFR1 antibodies.

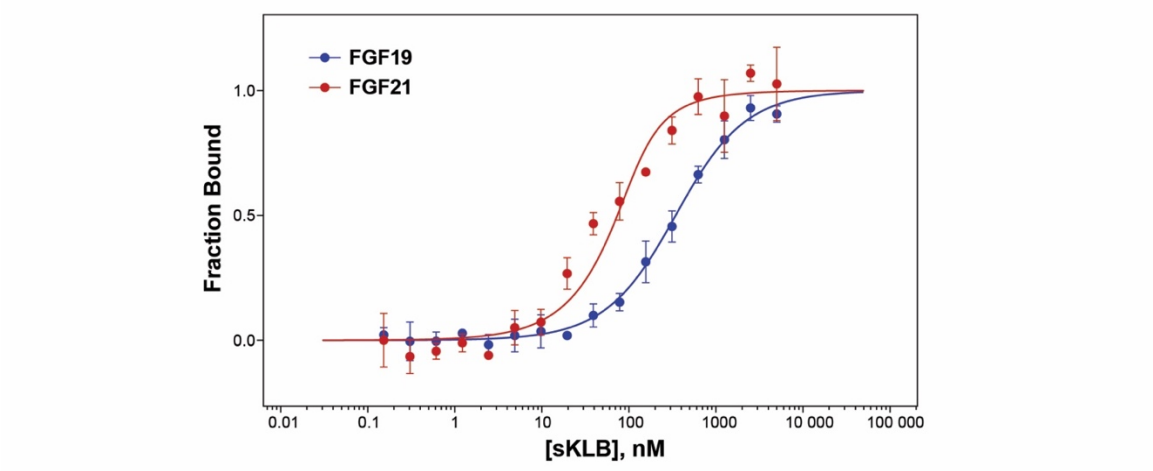

Fig. S4. Binding affinity measurements using MicroScale Thermophoresis (MST). N-terminal hexa-histidine tags on WT FGF19 and WT FGF21 were fluorescently labeled with RED-tris-NTA and mixed with a series of concentrations of sKLB. The thermophoretic movements of fluorescently labeled ligands in each sample were monitored and the normalized fluorescence intensities (FNorm) for each sample were plotted against the concentrations of sKLB. Fitting of the binding curves yielded dissociation constant K_D of 294 ± 27 nM and 23 ± 11 nM for FGF19-sKLB (blue) and FGF21-sKLB (red), respectively. The binding curves are normalized to the fraction of bound molecules for a better comparison. The dots and error bars for each graph denote means and variations of ΔFnorm (n = 3 independent samples).

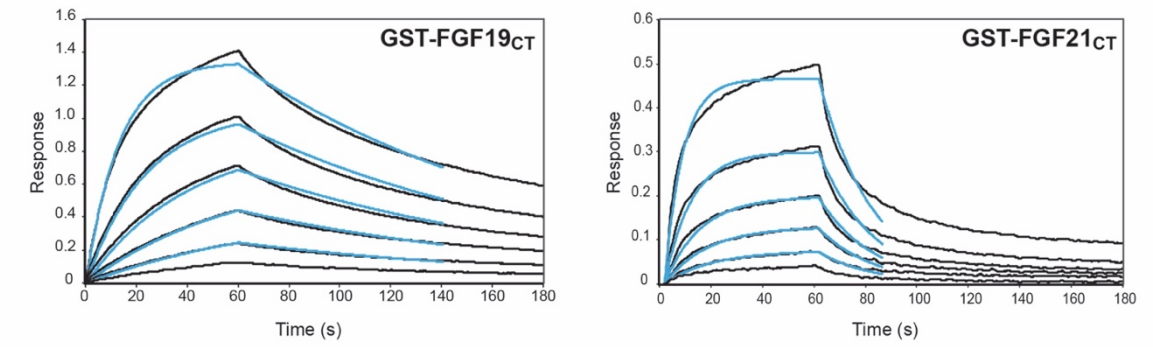

Fig. S5. BLI measurements of GST-FGF19$_{CT}$ and GST-FGF21$_{CT}$ to sKLB. GST-FGF19$_{CT}$ or GST-FGF21$_{CT}$ were immobilized on anti-GST sensors and dipped into solutions containing a series of concentrations of sKLB, ranging from 6.25 nM to 400 nM. Fitting the sensorgrams with 1:1 binding model yielded overall K_D of 211 ± 14 nM and 36.4 ± 2.3 nM (mean ± S.E.M. for 4 independent measurements) for GST-FGF19$_{CT}$ binding to sKLB and GST-FGF21$_{CT}$ binding to sKLB, respectively.

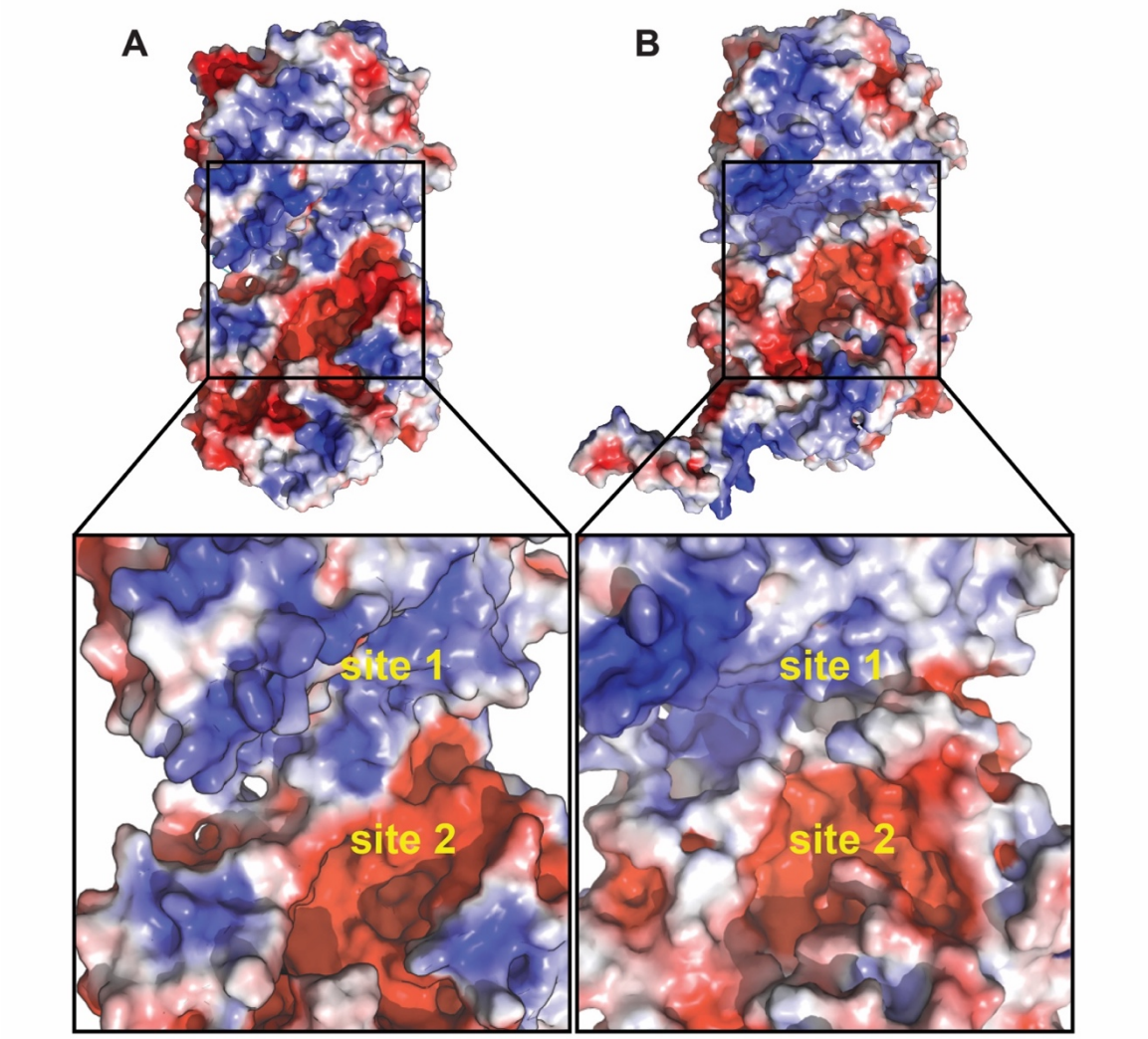

Fig. S6. Comparison of surface electrostatic potentials of sKLA model and sKLA structure. Comparison of surface electrostatic potentials of the (A) sKLA model based on sKLB:FGF21$_{CT}$ crystal structure (PDB ID: 5VAQ), and (B) sKLA from the crystal structure of sKLA:FGF23:FGFR1c$_{D2D3}$ complex (PDB ID: 5W21).

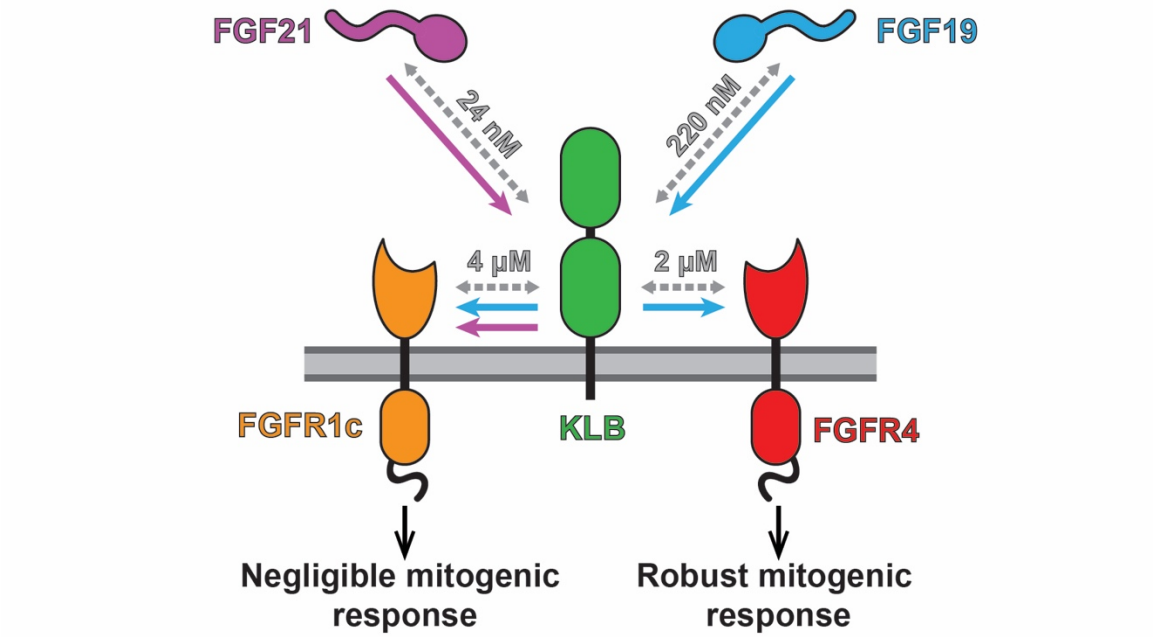

Fig. S7. Schematic diagram of molecular interactions involved in the FGF21 and FGF19 signaling. FGF19 and FGF21 bind to KLB with K_D of approximately 220 nM and 24 nM, respectively, and KLB binds to FGFR1 and FGFR4 with K_D of approximately 4 µM and 2 µM, respectively. The binding affinities of FGF19 and FGF21 to FGFR4 or FGFR1c are too weak to be reliably measured. Colored arrows indicate stimulatory activity of FGF21 (magenta) or FGF19 (light blue). FGF19 induces a robust mitogenic response and FGF21 induces a very weak mitogenic response when stimulating the same cells.

Table S1. Crystallographic data collection and refinement statistics

	sKLB:FGF19$_{CT}$:Nb30
Data collection	
Wavelength	0.9792
Space group	C2
Cell dimensions	
a, b, c (Å)	130.09, 143.9, 141.05
α, β, γ (°)	90, 90.90, 90
Resolution (Å)	58.71 - 3.20 (3.31 - 3.20)
CC1/2 (%)	98.2 (51.9)
$\langle I/\sigma \rangle$	3.40 (0.81)
Completeness (%)	99.23 (95.87)
Redundancy	3.8 (3.3)
Refinement	
No. reflections used	42869 (4112)
No. reflections used for R-free	1985 (188)
R_{work} / R_{free} (%)	27.96 (39.12) / 31.96 (40.99)
R.m.s. deviations	
Bond lengths (Å)	0.004
Bond angles (°)	0.94
Average B-factors	80.91

Table S2. Binding kinetics parameters of FGF19 and FGF21 variants to sKLB determined by bio-layer interferometry. All data are presented as mean values ± S.E.M from at least 3 independent experiments.

Construct	K_D ($\times 10^{-9}$ M)	k_{on} ($\times 10^{5}$ $M^{-1}s^{-1}$)	k_{off} ($\times 10^{-3}$ s^{-1})
FGF19	210±13	2.9±0.3	(6.1±0.7) ×10
FGF21	24.1±0.4	2.7±0.1	6.4±0.2
$FGF19_{21CT}$	37±3	2.4±0.1	9.0±0.8
$FGF19_{21site2}$	43±2	3.1±0.2	(1.4±0.1) ×10
$FGF21_{19site2}$	165±13	2.8±0.4	(4.6±0.2) ×10
$FGF19_{E193D}$	82±2	2.3±0.2	(1.6±0.3) ×10
$FGF19_{21site2W}$	22.2±1.2	2.3±0.2	5.4±0.4
$FGF21_{WF}$	5.2±0.6	3.4±0.7	1.7±0.1
$FGF19_{21CTWF}$	6.6±1.3	2.8±0.2	1.7±0.2

Movie S1. Movie illustrating inter-domain angle changes in crystal structures of various sKLB complexes. sKLB is shown as surface representation (red, KL1; blue, KL2). Nanobodies and ligands are omitted for clarity. The structures were overlaid with respect to KL1 and the trajectories between the coordinates were calculated using "morph" function in PyMOL.

References

1. Lee S*, et al.* (2018) Structures of beta-klotho reveal a 'zip code'-like mechanism for endocrine FGF signalling. *Nature* 553(7689):501-505.
2. Sali A & Blundell TL (1993) Comparative protein modelling by satisfaction of spatial restraints. J Mol Biol 234(3):779-815.
3. Shen MY & Sali A (2006) Statistical potential for assessment and prediction of protein structures. Protein Sci 15(11):2507-2524.
4. Baker NA, Sept D, Joseph S, Holst MJ, & McCammon JA (2001) Electrostatics of nanosystems: application to microtubules and the ribosome. Proc Natl Acad Sci U S A 98(18):10037-10041.
5. Dolinsky TJ, *et al.* (2007) PDB2PQR: expanding and upgrading automated preparation of biomolecular structures for molecular simulations. Nucleic Acids Res 35(Web Server issue):W522-525.